Hindawi
Advances in Astronomy
Volume 2022, Article ID 3255088, 13 pages
https://doi.org/10.1155/2022/3255088

Research Article

A High-Precision Dynamic Six Degree-of-Freedom Pose Measurement of the Subreflectors of Large Antennas Based on a Position Sensitive Detector and Laser Array

Shangmin Lin,[1,2] Wei Wang,[1] Hu Wang,[1,2] Yang Song,[1] Yue Pan,[1] Jiang Qiao,[1,2] Yaoke Xue,[1] Qinfang Chen,[1] Meiying Liu,[1,2] Yang Shen,[1] Jie Liu,[1] Yang Liu,[1] Yongjie Xie,[1] and Canglong Zhou[1]

[1]*Xi'an Institute of Optics and Precision Mechanics, Chinese Academy of Sciences, Xi'an 710119, China*
[2]*University of the Chinese Academy of Sciences, Beijing 100049, China*

Correspondence should be addressed to Hu Wang; wanghu@opt.ac.cn

Received 24 March 2022; Revised 27 May 2022; Accepted 16 June 2022; Published 5 July 2022

Academic Editor: Fernando Aguado Agelet

Subreflector misalignment of a large steerable radio telescope induces a pointing error and reduces the gain of the antenna system. To improve the antenna's operational efficiency, it is necessary to measure and adjust the position and attitude of the subreflector in real time. In this paper, a method based on a position sensitive detector (PSD) and laser array without an optical system is proposed to measure the six degree-of-freedom (DOF) poses of the subreflector. The laser emitted by the laser module array ensures that the PSD can be covered as it moves with the subreflector, and the PSD can obtain more than three laser beams. These ensure the measurement of all attitude changes of a large-aperture antenna subreflector. The two-dimensional coordinates of the centroids of three laser spots are extracted using the PSD, and then the bursa model is established to complete the coordinate transformation. Finally, the 6-DOF attitude information of the antenna subreflector is obtained. The results of a 6.05 m measurement simulation show that it can obtain high 6-DOF PSD attitude information. The experimental results show that the 6-DOF position and attitude information of the subreflector at a distance of 5.78 m can be obtained within seconds. Moreover, the error of the translation is within 0.014 mm and the error of the rotation is within 0.37°. This method can meet the pose measurement requirements of the subreflector.

1. Introduction

Given the rapid development of science and technology along with a desire to understand the mystery of the universe, humans are constantly looking deeper into the universe. The world's main space powers have invested large amounts of money and labor in space exploration. To observe the universe deeper and more clearly, large satellite antennas and large-aperture reflection antennas must be built [1–3].

In large-aperture reflection antennas, a large-caliber antenna subreflector adjustment mechanism is mounted on a support truss. During observation, it moves with the antenna's main reflector. Because the subreflector is connected to the main reflector via a support structure, the distance from the subreflector to the main reflector is usually very long; the mechanical model can be approximated as a cantilever beam. When it is deformed by gravity, wind, and temperature, the subreflector position will change, which causes antenna pointing and phase errors and ultimately results in a significant decrease in antenna efficiency at high and low elevations. To improve the observation performance of such telescopes, subreflector compensation techniques have been widely used in recent years. The subreflector is actively adjusted through a six degree-of-freedom (DOF) parallel mechanism to correct the position deviation,

Table 1: Summary of the main measurement techniques of the antenna subreflector.

Measurement scheme	Advantages	Weakness	Usage
Photogrammetry method	High accuracy (within 0.1 mm)	Dozens of hours-several days	Demarcate
Radio method	High accuracy (0.05 mm)	Dozens of minutes, specific signal source	Demarcate
Laser tracker	High accuracy (0.05 mm)	Accuracy of measurement decreases while the measuring distance increases	Demarcate

ensuring that it is at the best position relative to the antenna main plane under the day's working condition. Moreover, it has high spatial pose stability [4, 5].

Subreflector compensation has mainly been used in the American 100 m Green Bank Radio Telescope [6], German 100 m Effelsberg Radio Telescope, Italian 64 m Sardinia Radio Telescope (SRT), and the National Aeronautics and Space Administration's Deep Space Net series of antennas [7]. The Chinese 13.7 m Delingha Millimeter-wave Telescope [8] and 65 m Shanghai Radio Telescope also use movable subreflector compensation technology [9]. The highly accurate position control of the antenna is one of the key ways to ensure the high pointing accuracy of the radio telescope antenna, and the accurate measurement of the position of the subreflector is of great importance for its position control.

To improve the adjustment accuracy of the subreflector position under all working conditions, the measurement should be conducted in real time. At present, laser tracker, radio holography, photogrammetry-based, and other mature techniques are adopted to measure the position of the subreflector. These measurement schemes are summarized in Table 1.

In the 65 m radio telescope of the Shanghai Astronomical Observatory (TM 65 m), Hou et al. [10] used a laser tracer to calibrate the 80 m adjustment mechanism to determine the position of the subreflector, as shown in Figure 1. After calibration, the position accuracy was 0.108 mm, the posture accuracy was 9.72, and the highest position and posture errors decreased by 87.75% and 46%, respectively.

Wang et al. [11] used very long baseline interferometry based on the Chinese She Shan 25 m antenna and TM 65 m antenna to obtain the amplitude and phase of the caliber plane while the TM 65 m antenna scanned the neighborhood around 3C84. Then, the subreflector orientation was separated from the obtained aperture plane phase.

As shown in Figure 2, the 64 m SRT adopts a multiple analysis measurement system to determine the subreflector position, in which the laser measurement system can measure the position changes in four DOFs of the subreflector, with a measurement accuracy of $\pm 50\,\mu$m and $1''$ [12, 13].

Target attitude measurement techniques are used in industrial applications in other fields. For instance, Liu et al. designed a noncontact optical measurement system [14, 15] that can simultaneously measure the geometric error of six DOFs of the rotation axis of a machine tool. The method can measure six DOFs at a distance of more than 200 mm, and the measurement accuracy can reach micron and arc-second level. Laser triangulation [16] and optical frequency comb

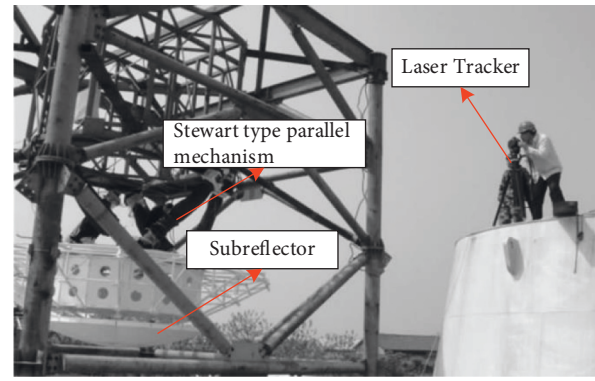

Figure 1: TM 65 m subreflector attitude measurement.

precision measurement [17] can often achieve micron-level measurement accuracy at relatively short distances, but it is difficult to achieve high-precision measurements in harsh environments with a distance of tens of meter. However, the development of these techniques is still very informative for measurement methods for the antennas.

The QiTai 110 m Radio Telescope (QTT), currently under construction in China, is fully steerable [18]. The large-aperture antenna adopts an adjustable Gregorian optical system design, and it will become one of the largest and most advanced all-round rotatable radio telescopes in the world. During the movement of the antenna, the subreflector position will be severely affected by the environmental load. However, movable subreflector active compensation to improve the work efficiency of the antenna system is also a key part in the QTT project. This requires improving the adjustment accuracy of the subreflector under all working conditions, and its position needs to be detected in real time and with high-precision.

The existing measurement scheme does not meet the requirements of QTT position measurement. The photogrammetry-based method is used to calibrate the position of the system in the antenna construction stage because of the slow speed of image acquisition and calculation; hence, it cannot be used during the antenna's operation. In addition, a laser tracker can only be used in certain measurement environments. It is not suitable for long-term continuous measurement, and hence it cannot be used for the real-time measurement of the large-caliber antenna. Using cooperative targets over the long-term also reduces the accuracy because of the influence of the external environment. The measurement system used in the joint test scheme on the SRT can measure only five DOFs, that is not sufficient. Therefore, for the high-precision measurement of the QTT

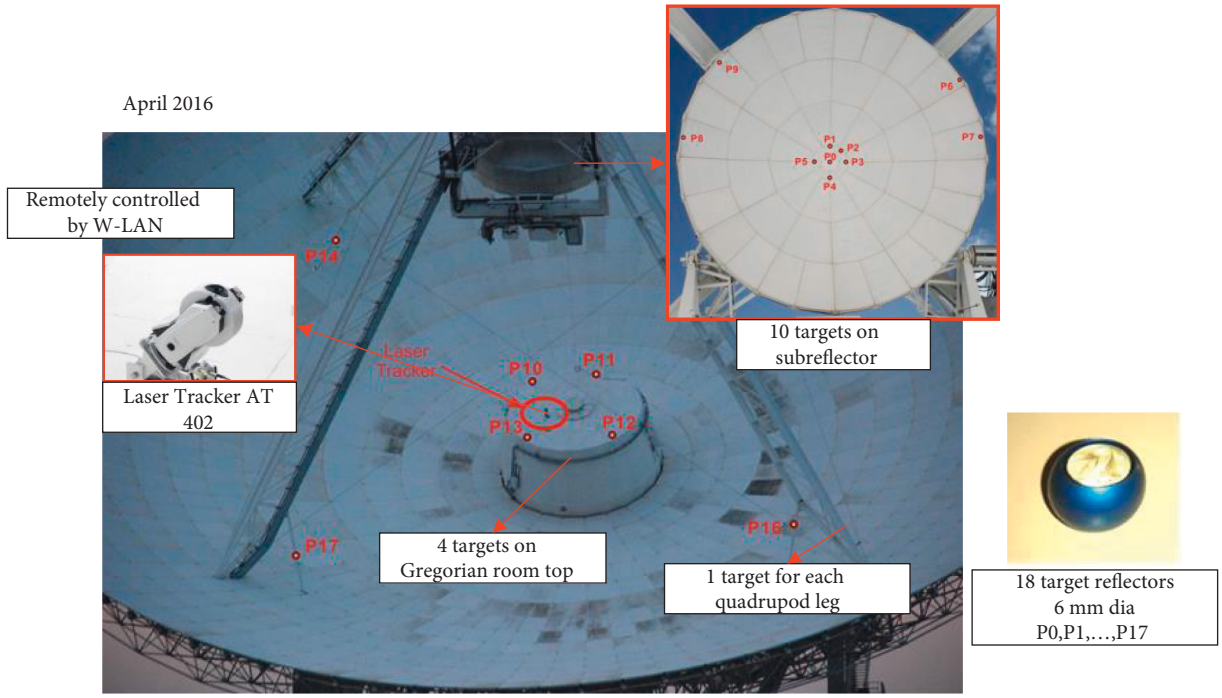

Figure 2: SRT measurement in Italy.

subreflector position, a new rapid measurement scheme needs to be developed.

This paper presents a triangulation technique using laser array coverage based on a position sensitive detector (PSD). The main contents of this paper are as follows: in the second section, the measurement scheme using a laser array to cover the subreflector is introduced. The third section describes how the least squares method is used to fit the spatial straight line of the laser beam and the distance of the PSD two-dimensional laser spot triangular centroid is used to obtain the three-dimensional spatial coordinates of the spot centroid. The 6-DOF attitude information of the antenna subreflector is obtained by coordinate conversion through the model. The fourth section verifies the feasibility and accuracy of this scheme through experiments. The final section concludes the paper.

2. Measurement Scheme

To detect the deformation of the QTT subreflector induced by factors in the environment such as wind, heat, and gravity in order to use the movable subreflector active compensation technique, it is necessary to accurately and quickly measure the position and attitude of the subreflector. QTT is a Gregorian antenna. The feed cabin is fixed relative to the origin of the central position of the main reflector. The subreflector is fixed by the support frame, which is supported by a driving mechanism for pose adjustment. The aperture of the subreflector is smaller than that of the antenna system, especially the main reflector, and hence the subreflector can be regarded as a rigid body when measuring the subreflector posture. Moreover, its posture can be represented by the posture of the PSD installed on the subreflector. In the method proposed in this paper, the laser array group is placed at the center of the main reflector, and PSD is installed to receive the laser beam in order to form a spot array on the subreflector and ensure that the laser beam emitted by the laser array group can cover the PSD, which moves with the subreflector, as shown in Figure 3. This scheme of laser coverage is suitable for a wide range of subreflector attitude change measurements.

By analyzing the two-dimensional position change of multiple light spots on the PSD, we can quickly obtain the three-dimensional coordinates of the spatial position of the subreflector relative to the center of the main reflector, realizing the closed-loop control of the position and attitude of the antenna subreflector. The deformation of the antenna subreflector caused by gravity, sunshine, and wind load can be corrected in real time, realizing the active compensation of the system.

After the laser module has adjusted its pose, it forms an emission array aimed at the PSD on the subreflector. The spatial information of the outgoing laser beam close to the subreflector measurement section is calibrated in advance to ensure that the laser beam array formed by multiple sets of lasers can cover the motion range of the PSD with the subreflector and the PSD can always observe enough laser spots, as shown in Figure 4.

A group of laser beams are emitted from the laser array, of which at least three laser beams are irradiated onto the PSD. This enables the linear equation of the space laser where the three light spots on the PSD are located for identification. The current operation of the antenna attitude change shows that the attitude change of the antenna is mainly due to position error during pitch motion [19], and hence the beams can be identified by the movement of the

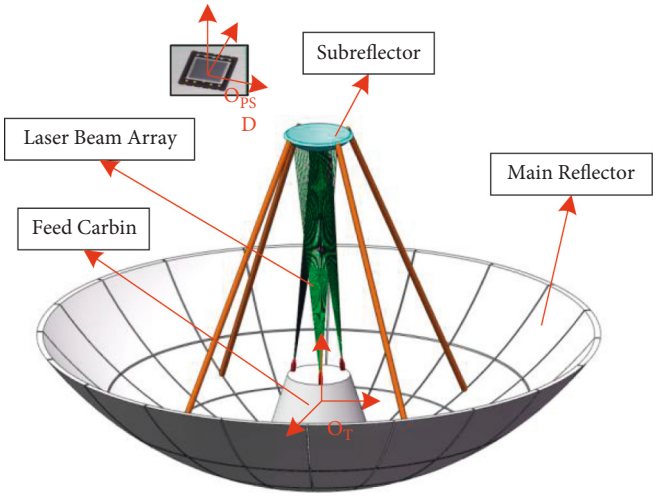

Figure 3: Schematic diagram of the laser array and PSD installation position.

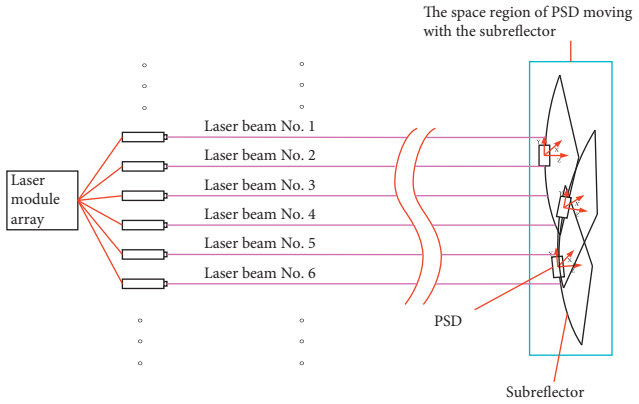

Figure 4: Schematic diagram of the motion space of the laser array and detector.

three light spots on the shading plate. Then, the three-dimensional space coordinates of the light spots are calculated according to the distances between them, as captured by the PSD, and the pose of the secondary surface can be obtained, as shown in Figures 5 and 6. The test workflow of the laser measurement system is shown in Figure 7.

3. Measurement Principle

In the method proposed in this paper, the motion range of the measured target point is covered by the laser array, and the attitude information of the point target is obtained using the principle of a spatial geometric coordinate transformation of the location where the spatial straight line intersects the target surface of the detector.

4. Line Fitting of the Laser Beam

The three-dimensional information of the discrete points of the laser spot is obtained from the premeasured PSD

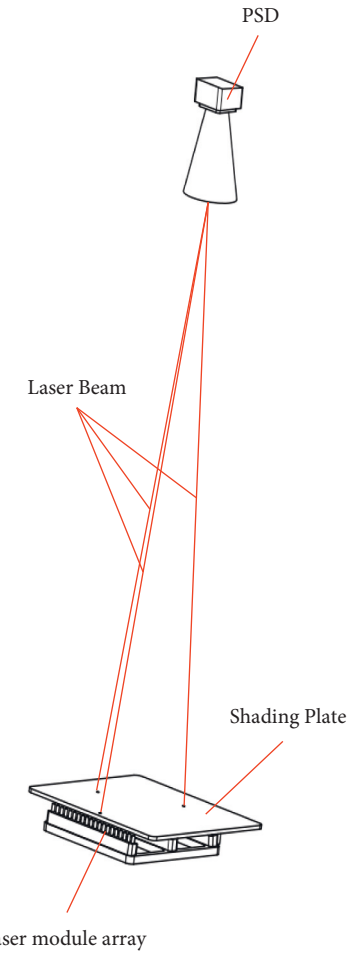

Figure 5: Schematic diagram of the laser module array emission beam.

translation information, the two-dimensional spot information is obtained by the actual measurement, and then the three spatial straight lines of the emitted laser beam are fitted by the principle of least squares [20].

The spatial linear equation can be expressed as follows:

$$\begin{cases} x = a_1 z + a_2, \\ y = b_1 z + b_2, \\ z = z. \end{cases} \tag{1}$$

Here, (x, y, z) denotes the three-dimensional coordinates of the centroid space of the spot formed by the intersection of a laser beam and the PSD; a_1, a_2, b_1, and b_2 are linear equation constants.

Equation (1) can also be expressed as follows:

$$\begin{bmatrix} a_1 & a_2 \\ b_1 & b_2 \end{bmatrix} \begin{bmatrix} z \\ 1 \end{bmatrix} = \begin{bmatrix} x \\ y \end{bmatrix}. \tag{2}$$

Then, the coordinates of N discrete points are expressed as follows:

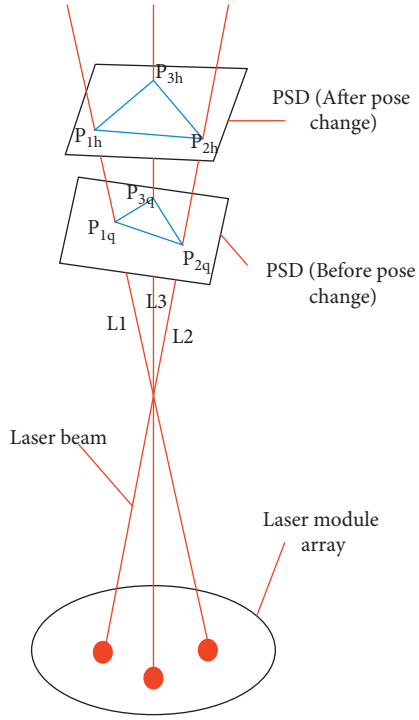

Figure 6: Schematic principle of the subreflector measurement system.

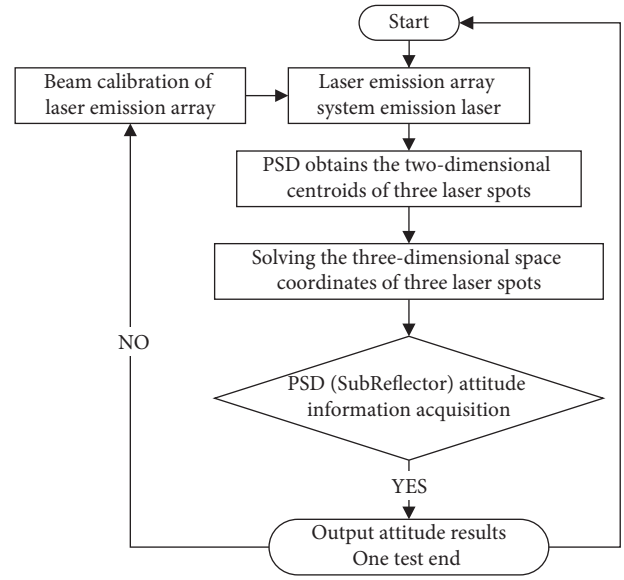

Figure 7: Test workflow of the laser measurement system.

$$\begin{bmatrix} a_1 & a_2 \\ b_1 & b_2 \end{bmatrix} \begin{bmatrix} z_1 & \cdots & z_n \\ 1 & \cdots & 1 \end{bmatrix} \begin{bmatrix} z_1 & \cdots & z_n \\ 1 & \cdots & 1 \end{bmatrix}^T = \begin{bmatrix} x_1 & \cdots & x_n \\ y_1 & \cdots & y_n \end{bmatrix} \begin{bmatrix} z_1 & \cdots & z_n \\ 1 & \cdots & 1 \end{bmatrix}^T, \tag{3}$$

$$\begin{bmatrix} a_1 & a_2 \\ b_1 & b_2 \end{bmatrix} \begin{bmatrix} \sum_1^n z_i^2 & \sum_1^n z_i \\ \sum_1^n z_i & n \end{bmatrix} = \begin{bmatrix} \sum_1^n x_i z_i & \sum_1^n x_i \\ \sum_1^n y_i z_i & \sum_1^n y_i \end{bmatrix}, \tag{4}$$

$$\begin{bmatrix} a_1 & a_2 \\ b_1 & b_2 \end{bmatrix} = \begin{bmatrix} \sum_1^n x_i z_i & \sum_1^n x_i \\ \sum_1^n y_i z_i & \sum_1^n y_i \end{bmatrix} \begin{bmatrix} \sum_1^n z_i^2 & \sum_1^n z_i \\ \sum_1^n z_i & n \end{bmatrix}^{-1}. \tag{5}$$

Finally, the following three linear equations of the emitted beam of the laser group are obtained:

$$\begin{cases} x_1 = z_1 a_{11} + a_{21}, \\ y_1 = z_1 b_{11} + b_{21}, \\ z_1 = z_1, \end{cases} \tag{6}$$

$$\begin{cases} x_2 = z_2 a_{12} + a_{22}, \\ y_2 = z_2 b_{12} + b_{22}, \\ z_2 = z_2, \end{cases} \tag{7}$$

$$\begin{cases} x_3 = z_3 a_{13} + a_{23}, \\ y_3 = z_3 b_{13} + b_{23}, \\ z_3 = z_3. \end{cases} \tag{8}$$

Here, (x_i, y_i, z_i) denotes the spatial coordinates of the centroid of the scattered light spot on the i-th laser beam and a_{1i}, a_{2i}, b_{1i}, and b_{2i} are the constant parameters of the linear equation, where $i = 1$, 2, and 3.

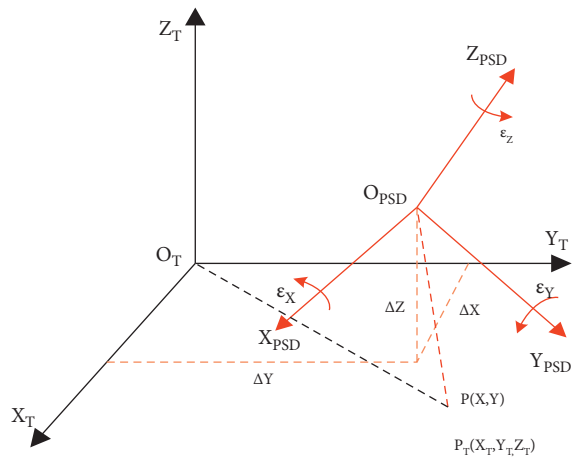

Figure 8: PSD coordinate system, space Euclidean coordinate system, and their transformation.

5. Solving for Intersecting Spot Centroid Coordinates

The two-dimensional coordinates of the centroid of the detector spot before the subreflector pose change are defined as P_{01}: (x_{01}, y_{01}), P_{02}: (x_{02}, y_{02}), and P_{03}: (x_{03}, y_{03}).

The three-dimensional coordinates of the centroid of the spot before the subreflector pose change are defined as P_{q01}: $(x_{q01}, y_{q01}, z_{q01})$, P_{q02}: $(x_{q02}, y_{q02}, z_{q02})$, and P_{q03}: $(x_{q03}, y_{q03}, z_{q03})$.

The two-dimensional coordinates of the centroid of the detector spot after the subreflector pose change are defined as P'_{01}: (x'_{01}, y'_{01}), P'_{02}: (x'_{02}, y'_{02}), and P'_{03}: (x'_{03}, y'_{03}).

Finally, the three-dimensional coordinates of the centroid of the spot after the subreflector pose change are defined as P_{h01}: $(x_{h01}, y_{h01}, z_{h01})$, P_{h02}: $(x_{h02}, y_{h02}, z_{h02})$, and P_{h03}: $(x_{h03}, y_{h03}, z_{h03})$.

Because the space line segments are equal in length, we have the following:

$$\left(x_{q01} - x_{q02}\right)^2 + \left(y_{q01} - y_{q02}\right)^2 + \left(z_{q01} - z_{q02}\right)^2 = \left(x_{02} - x_{01}\right)^2 + \left(y_{02} - y_{01}\right)^2, \tag{9}$$

$$\left(x_{q03} - x_{q03}\right)^2 + \left(y_{q03} - y_{q02}\right)^2 + \left(z_{q03} - z_{q02}\right)^2 = \left(x_{02} - x_{03}\right)^2 + \left(y_{02} - y_{03}\right)^2, \tag{10}$$

$$\left(x_{q03} - x_{q01}\right)^2 + \left(y_{q03} - y_{q01}\right)^2 + \left(z_{q03} - z_{q01}\right)^2 = \left(x_{01} - x_{03}\right)^2 + \left(y_{01} - y_{03}\right)^2. \tag{11}$$

Solving Equations (6)–(11), the three-dimensional coordinates of the PSD intersection points before the pose change of the subreflector can be obtained from the following intersection point coordinates on the PSD: P_{q01}: $(x_{q01}, y_{q01}, z_{q01})$, P_{q02}: $(x_{q02}, y_{q02}, z_{q02})$, and P_{q03}: $(x_{q03}, y_{q03}, z_{q03})$.

Similarly, the spatial three-dimensional coordinates of the PSD intersection point after the subreflector pose change can also be obtained as P_{h01}: $(x_{h01}, y_{h01}, z_{h01})$, P_{h02}: $(x_{h02}, y_{h02}, z_{h02})$, and P_{h03}: $(x_{h03}, y_{h03}, z_{h03})$.

6. PSD Pose Acquisition with Six DOFs

In this paper, the Bursa model [21] is employed to analyze the 7-parameter transformation from the two-dimensional coordinates of the PSD spot centroid to the three-dimensional coordinates of the antenna system space coordinate system. The translation and rotation data of the PSD reflect the 6-DOF attitude change information.

As shown in Figure 8, the two-dimensional coordinate points of the spot centroid on the PSD can be converted into three-dimensional spatial coordinate points under the antenna spatial coordinate system through translation and rotation as follows:

$$P_T = \Delta P + (1 + k)R(\varepsilon)P. \tag{12}$$

Here, $P_T = \left(X_T \;\; Y_T \;\; Z_T\right)^T$ denotes the three-dimensional coordinates of the light spot in the antenna coordinate system; ΔP is the translation vector $\Delta P = \left(\Delta X \;\; \Delta Y \;\; \Delta Z\right)^T$; k is the scale change coefficient; $R(\varepsilon)$ is the rotation matrix; and $P = \left(X \;\; Y \;\; Z\right)^T$ denotes the coordinates of the light spot in the PSD coordinate system, where $Z = 0$.

$$R(\varepsilon) = R(\varepsilon_Z)R(\varepsilon_Y)R(\varepsilon_X) = \begin{bmatrix} 1 & \varepsilon_Z & -\varepsilon_Y \\ -\varepsilon_Z & 1 & \varepsilon_X \\ \varepsilon_Y & -\varepsilon_X & 1 \end{bmatrix}. \tag{13}$$

Equation (12) can be transformed into the following:

Table 2: Initial conditions of the simulation calculations.

Simulation conditions	Parameter		
Coordinates of the exit points of the three laser beams (mm)	(−300, −200, 6000)	(300, −200, 6000)	(0, 200, 6000)
Second coordinate points of the three laser beams (mm)	(0, 0, 0)	(0, 0, 0)	(0, 0, 0)
Initial position of PSD target plane (mm)		$Z = 50$	
PSD attitude translation distance (mm)	1	0.5	1.5
PSD attitude deflection angle (degrees)	3	2	4

Table 3: Simulation results.

Solution step	Results		
Linear equations of the laser beams	$l1$: $x1 = -0.05z1$; $y1 = -0.0333z1$; $z1 = z1$;	$l1$: $x2 = 0.05z2$; $y2 = -0.0333z2$; $z2 = z2$;;	$l2$: $x3 = 0$; $y3 = 0.0333$; z3; $z3 = z3$;
Space coordinates of the centroid of the actual laser intersection spot (mm)	(−2.7575, −1.8383, 55.1500)	(2.7469, −1.8312, 54.9385)	(0, 1.8409, 55.2274)
Three solved coordinates of the centroid of the light spots (mm)	(−2.7575, −1.8383, 55.1500)	(2.7469, −1.8312, 54.9385)	(0, 1.8409, 55.2274)
PSD attitude translation results (mm)	0.9891	0.4918	1.4960
PSD attitude deflection results (degrees)	2.9968	1.9996	3.9547
Translation deviation (mm)	−0.0109	−0.0082	−0.0040
Deflection deviation (degrees)	−0.0032	−0.0004	−0.0453

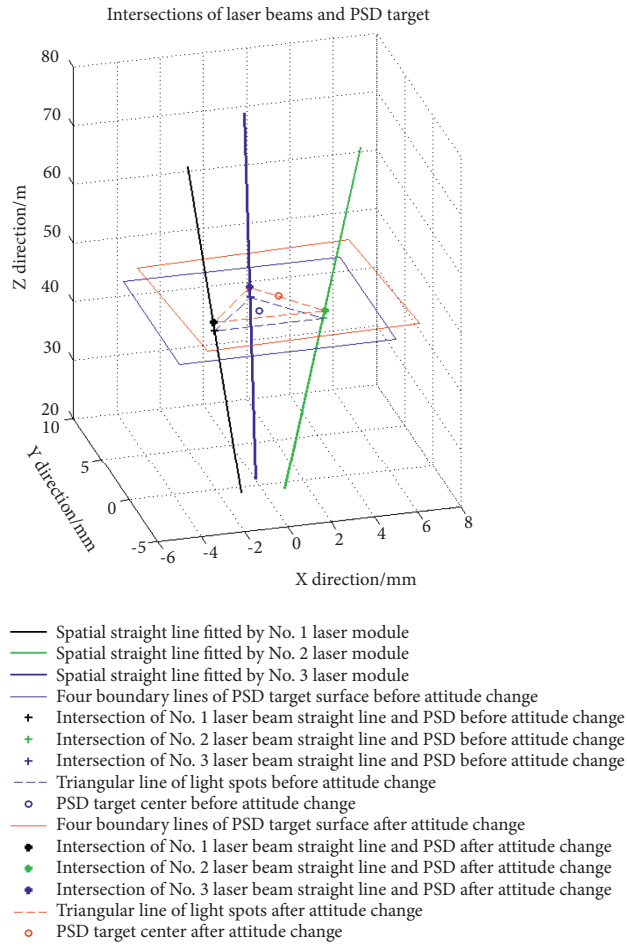

Figure 9: Intersection between the PSD and laser beams before and after attitude changes.

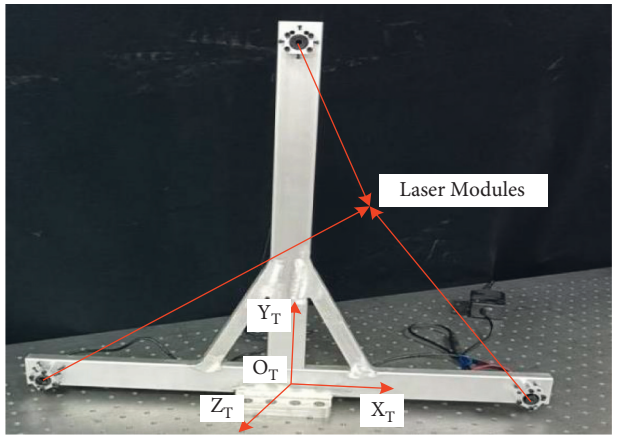

Figure 10: Laser emission system.

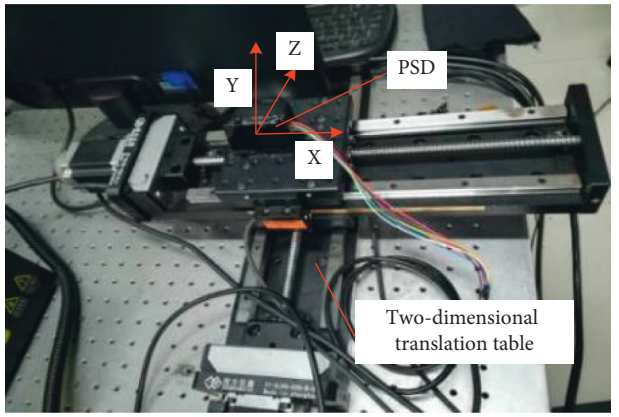

Figure 11: PSD and two-dimensional translation table.

$$\begin{bmatrix} X_T \\ Y_T \\ Z_T \end{bmatrix} = \begin{bmatrix} \Delta X \\ \Delta Y \\ \Delta Z \end{bmatrix} + (1+k) \begin{bmatrix} 1 & \varepsilon_z & -\varepsilon_Y \\ -\varepsilon_z & 1 & \varepsilon_X \\ \varepsilon_Y & -\varepsilon_X & 1 \end{bmatrix} \begin{bmatrix} X \\ Y \\ Z \end{bmatrix}. \quad (14)$$

The centroid coordinates of the three light spots in the spatial coordinate system of the antenna system are defined as $P_{Ti} = (X_{Ti}\ Y_{Ti}\ Z_{Ti})^T\ i = 1, 2, 3$. The coordinates of the corresponding three points in the PSD coordinate system are defined as $P_i = (X_i\ Y_i\ Z_i)^T$, $i = 1, 2, 3$. Then, equation (14) can be further expressed as follows:

$$\begin{bmatrix} X_{Ti} - X_i \\ Y_{Ti} - Y_i \\ Z_{Ti} - Z_i \end{bmatrix} = \begin{bmatrix} 1 & 0 & 0 & X_i & 0 & -Z_i & Y_i \\ 0 & 1 & 0 & Y_i & Z_i & 0 & -X_i \\ 0 & 0 & 1 & Z_i & -Y_i & X_i & 0 \end{bmatrix} \begin{bmatrix} \Delta X \\ \Delta Y \\ \Delta Z \\ k \\ \varepsilon_X \\ \varepsilon_Y \\ \varepsilon_Z \end{bmatrix}. \quad (15)$$

Using the least squares method, the transformation matrix of multiple groups of points in different coordinate systems can be solved. The solution is defined as follows:

Table 4: Experimental PSD parameters.

Parameter	Value
PSD type	Two-dimensional PSD
Model	PSD100-SPB
Active sensor area	10 mm × 10 mm
Resolution ratio	1 μm
Work frequency	10 Hz
Maximum work efficiency spectrum segment	780 nm

Table 5: Laser module parameters.

Parameter	Value
Light spectrum	760 nm
Power	5 mw
Spot size (6 m)	2 mm

$$\alpha_i = \begin{bmatrix} X_{Ti} - X_i \\ Y_{Ti} - Y_i \\ Z_{Ti} - Z_i \end{bmatrix}, \quad i = 1, 2, 3,$$

$$A = (\alpha_1, \alpha_2, \alpha_3)^T,$$

$$m_i = \begin{bmatrix} 1 & 0 & 0 & X_i & 0 & -Z_i & Y_i \\ 0 & 1 & 0 & Y_i & Z_i & 0 & -X_i \\ 0 & 0 & 1 & Z_i & -Y_i & X_i & 0 \end{bmatrix}, \quad i = 1, 2, 3,$$

$$M = (m_1, m_2, m_3)^T,$$

$$B = [\Delta X\ \ \Delta Y\ \ \Delta Z\ \ k\ \ \varepsilon_X\ \ \varepsilon_Y\ \ \varepsilon_Z]^T,$$

$$A = \mathrm{MB} \quad (16)$$

$$\cdot \frac{\partial (A - \mathrm{MB})^T (A - \mathrm{MB})}{\partial B}$$

$$= 2 \frac{\partial (A - \mathrm{MB})^T}{\partial B} (A - \mathrm{MB})$$

$$= 2 \frac{\partial \left(A^T - B^T M^{\mathrm{T}}\right)}{\partial B} (A - \mathrm{MB})$$

$$= 2 \left(\frac{\partial A^T}{\partial B} - \frac{\partial \left(B^T M^T\right)}{\partial B} \right) (A - \mathrm{MB})$$

$$= -2M^T (A - \mathrm{MB})$$

$$= -2M^T A + 2M^T, \quad \mathrm{MB} = 0.$$

$$B = \left(M^T M\right)^{-1} M^T A. \quad (17)$$

By solving the 6-DOF coordinate change in PSD in space, the change in the subreflector pose can finally be obtained.

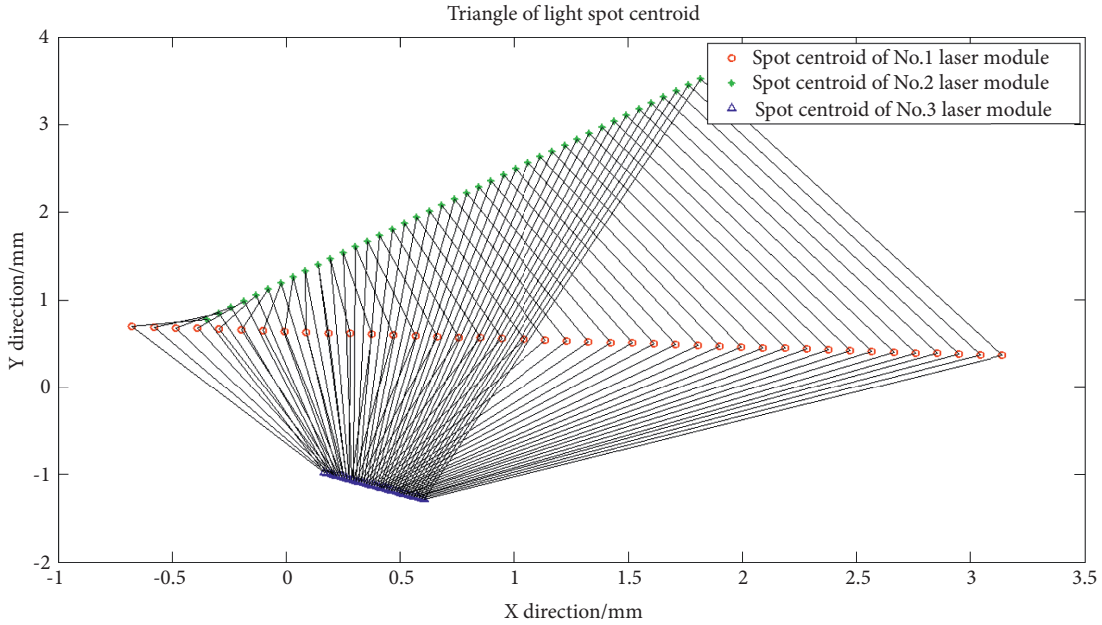

Figure 12: Forty-one sets of experimental data of three-dimensional coordinates of the spot centroid obtained by the PSD.

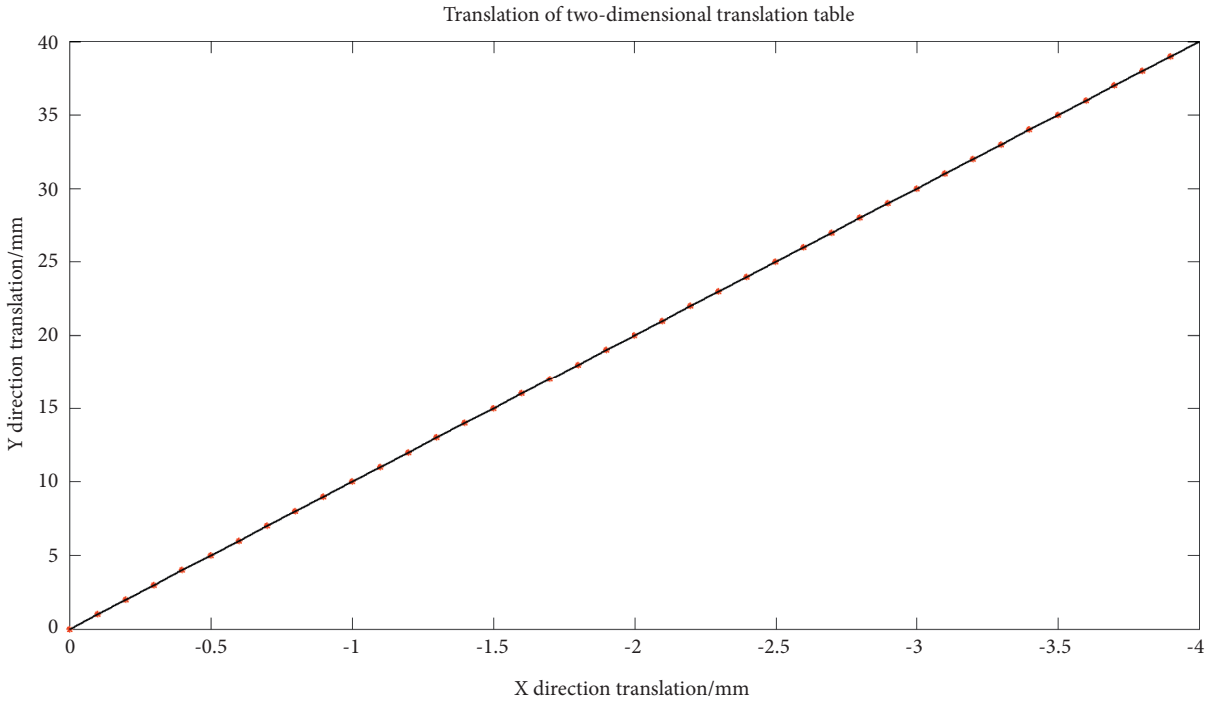

Figure 13: Translation of the two-dimensional translation table in the X and Z directions.

7. Simulation Example

To evaluate the measurement principle, a simulation of an example was performed. Three emission lasers were set to irradiate on a PSD target surface 6.05 m away. The PSD attitude was given a predetermined offset, and the change in attitude was calculated using the method proposed in the previous section, and the results were compared with the predetermined offset.

The initial conditions are shown in Table 2.

Using the spatial coordinates of two points of any laser beam, three laser line equations can be obtained. Then, the two-dimensional coordinates of the three light spots can be obtained directly by the PSD and the three-dimensional

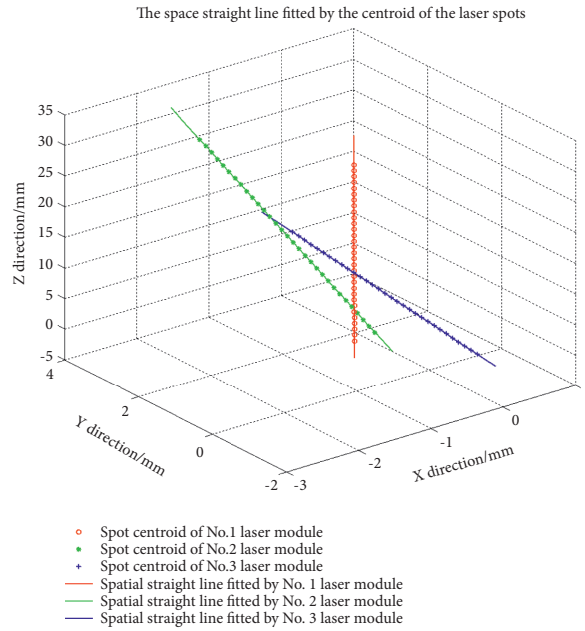

Figure 14: Three fitted laser beams.

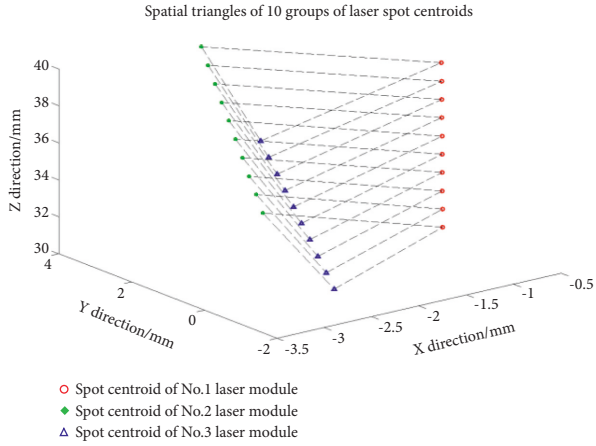

Figure 15: Calculated spatial coordinates of the last 10 sets of spot centroids.

coordinates of three light spots can be obtained by Equations (9)–(11). Finally, the bursa model is established, and the change in attitude of the PSD is obtained by Equation (17). The results are shown in Table 3. A schematic diagram of interaction between the PSD and laser beams before and after the attitude changes is shown in Figure 9.

The results in Table 3 show that the proposed method in the simulation example obtains the three-dimensional coordinates of spatial laser spots with high accuracy and obtains the final 6-DOF change in attitude of the PSD with high accuracy.

8. Experiment

To further evaluate the measurement scheme, a prototype measurement system was built to simulate the attitude adjustment of the antenna. It mainly consists of a laser emission module array, PSD system, and two-dimensional translation platform. The laser module array is placed on the aluminum support frame, and the PSD system is placed on the two-dimensional movable table. The experimental equipment settings are shown in Figures 10 and 11. The main equipment parameters are shown in Tables 4 and 5.

The 41 groups of data obtained from the experiment are shown in Figure 12, and the corresponding 41 groups of translation in X direction and Z direction are shown in Figure 13.

The first 31 sets of data were used to fit the laser beam straight lines as shown in Figure 14, and the last 10 sets of data were used to test and evaluate the system.

The first 31 sets of data obtained were processed using Equations (5)–(8), and the three space linear equations were fitted as follows:

$$L1: \begin{cases} x_1 = -0.0046z_1 - 0.6748, \\ y_1 = -0.0084z_1 + 0.7011, \\ z_1 = z_1, \end{cases} \tag{18}$$

$$L2: \begin{cases} x_2 = -0.0458z_2 - 0.3491, \\ y_2 = 0.0684z_2 + 0.7816, \\ z_2 = z_2, \end{cases} \tag{19}$$

$$L3: \begin{cases} x_3 = -0.0891z_3 + 0.1662, \\ y_3 = 0.0076z_3 + 0.9772, \\ z_3 = z_3. \end{cases} \tag{20}$$

Taking the two-dimensional information obtained from the last 10 groups data as variables, Equations (18)–(20) and (9)–(11) were used to solve the space centroid coordinates of the spot where the PSD and lasers intersected. The results are

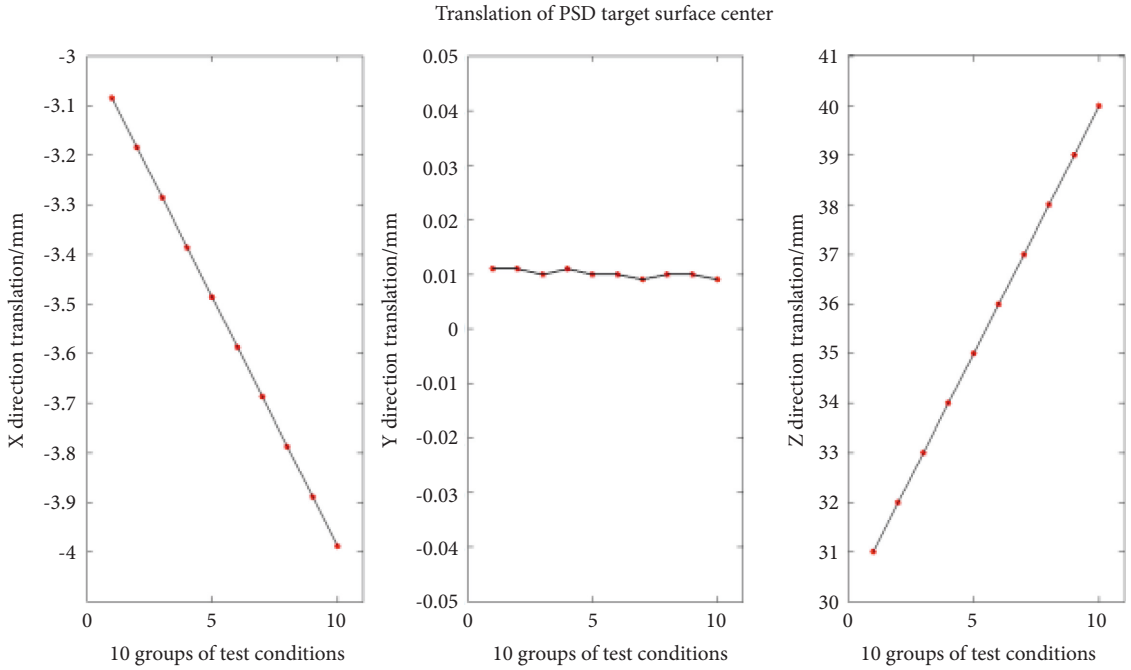

Figure 16: Results of the last 10 groups of change in the 3-DOF PSD translation.

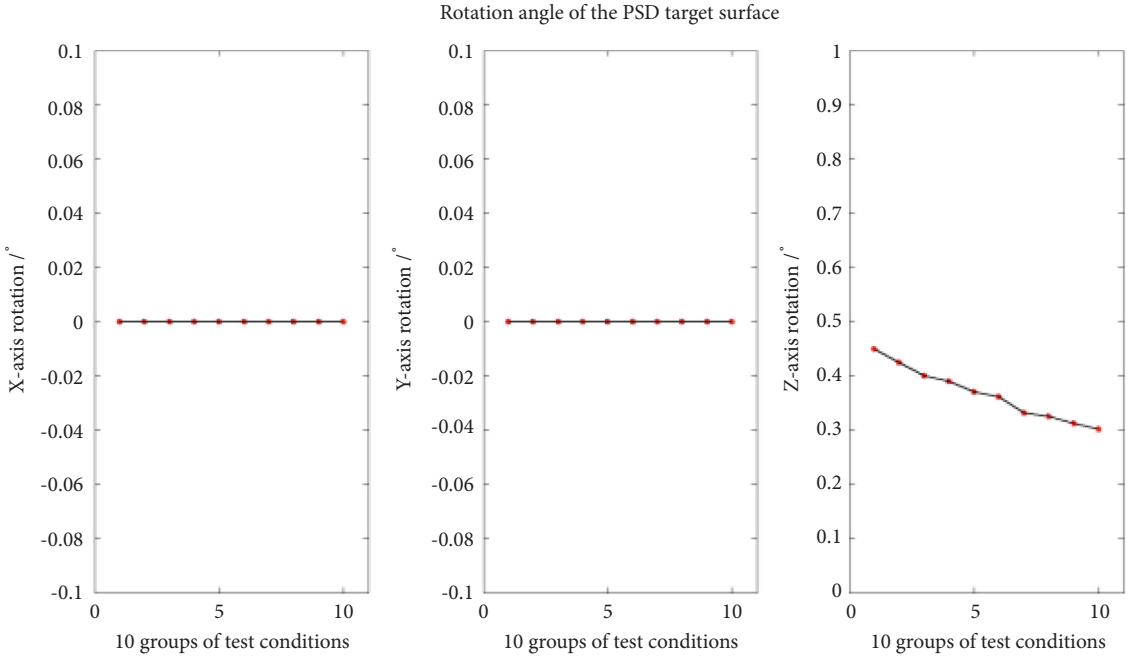

Figure 17: Results of the last 10 groups of change in the 3-DOF PSD rotation.

shown in Figure 15. The selected high-precision two-dimensional translation table is equipped with a high-precision RH100 × 30D05 A grating ruler (Renishaw, UK), with an accuracy of 1 μm. Therefore, the data from the motion of the two-dimensional translation platform can be used as the actual translation of the PSD, and the measurement accuracy can be obtained by comparing it with the solved change in attitude. Finally, the 6-DOF change in the subreflector position was obtained from Equations (15)–(17) as shown in Figures 16 and 17.

The change in PSD attitude caused by the two-dimensional translation table consisted of translation in the X and Z directions without rotation. The solved maximum translation root mean squared (RMS) error was 0.014 mm, and the maximum rotation RMS error was 0.370°, as shown in Figures 18 and 19.

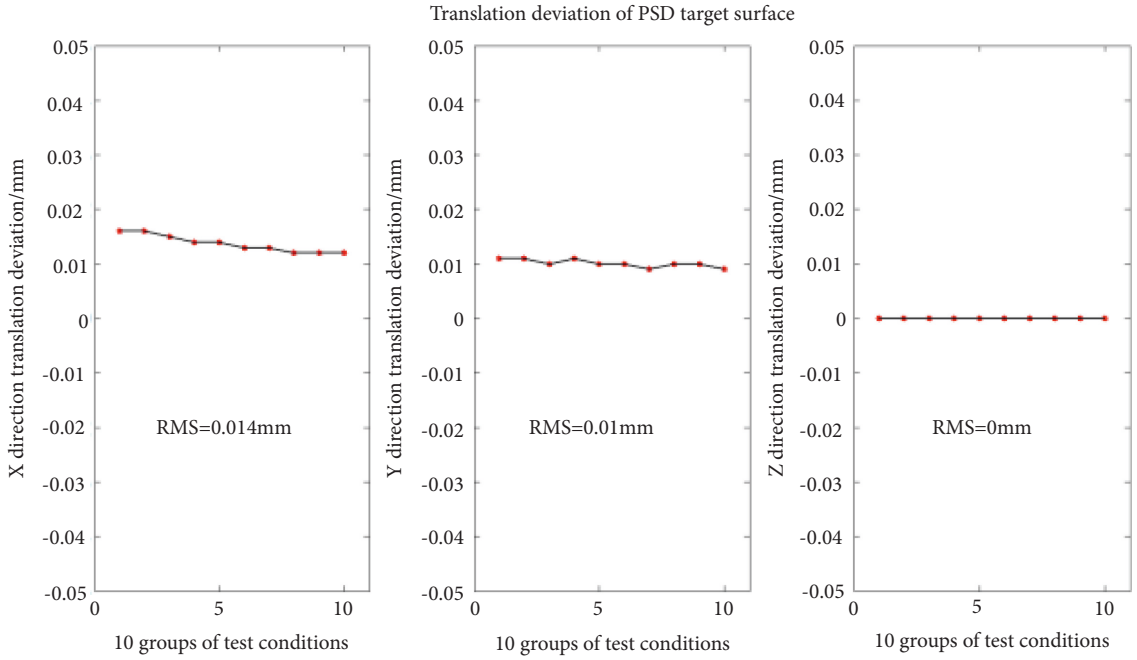

Figure 18: Last 10 groups of the PSD 3-DOF attitude translation errors.

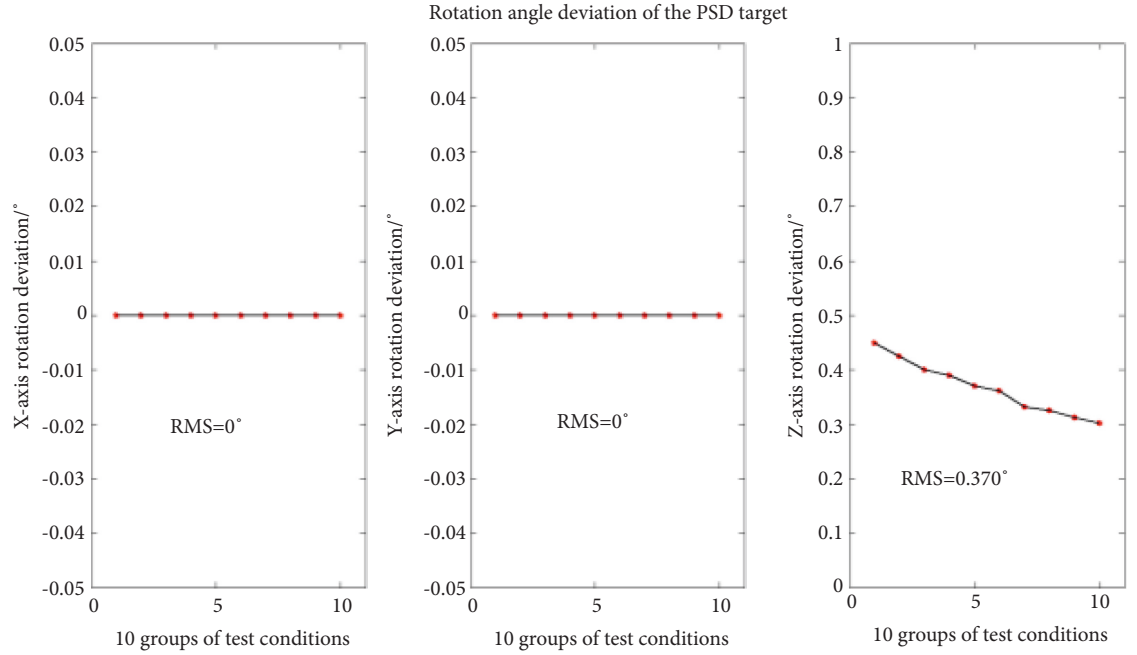

Figure 19: Last 10 groups of PSD 3-DOF attitude rotation errors.

In this experiment, the two-dimensional coordinate output operating frequency of PSD was 10 Hz, and the runtime of the measurement system's algorithm was on the order of milliseconds, and hence the time needed for system measurement can be guaranteed to be within several seconds. The results of this verification experiment prove that the measurement scheme proposed in this paper is feasible and can be used for rapid and high-precision subreflector position measurement.

9. Conclusion

This paper focused on the fast and high-precision pose measurements of a large-caliber antenna subreflector and proposed a PSD-based triangulation technique for laser array coverage. The precalibrated laser array is mounted on the subreflector so that the PSD always observes at least three different laser beams and at least three complete laser spots are formed. The PSD can rapidly acquire the two-

dimensional centroid coordinates of the light spots by solving the spot centroid space coordinates using the three two-dimensional point distances and the laser beam line equation. Then, the coordinate transformation matrix can be obtained by the bursa model. Finally, the 3-DOF translation information and 3-DOF rotation information of the PSD can be obtained. Experimental results showed that a translation accuracy of 0.014 mm and a rotation accuracy of 0.37° can be achieved. In the future, we will devote ourselves to using detector array for research to further improve the measurement accuracy. Moreover, the proposed method can also meet the requirements of quasi-real-time subreflector position measurement. Using this technique, the antenna subreflector can be moved to the optimal position to improve antenna electrical performance and observation efficiency. This will be beneficial for obtaining high quality observation data and help humans explore the mystery of the universe.

Data Availability

Data underlying the results presented in this paper are not publicly available at this time but may be obtained from the authors upon reasonable request.

Conflicts of Interest

The authors declare that there are no conflicts of interest.

Acknowledgments

This study was supported by National Key Research and Development Program of China (grant no. 2021YFC2203501) and National Natural Science Foundation of China (NSFC) (grant no. 11803075).

References

[1] Y. Pang, "Key technologies of large antenna mechanical design," *Electro-Mechanical Engineering*, vol. 27, no. 3, pp. 28–30, 2011.

[2] H. F. Guo, "China's "sky eye" —five-hundred-meter aperture spherical radio telescope," *Military Digest*, vol. 7, no. 16, pp. 52–55, 2021.

[3] J. Q. Chen, *Principle and Design of Astronomical Telescope*, Nanjing University Press, Jiangsu, China, 2020.

[4] G. J. Leng, W. Wang, B. Y. Duan, and X. P. Li, "Subreflector real-time compensation for main reflector deformation of shaped Cassegrain antenna," *Systems Engineering and Electronics*, vol. 33, no. 5, pp. 996–1000, 2011.

[5] D. H. Yang, Y. Cheng, C. C. Wu, and Z. Y. FeiJin, "A novel hexapod and its prototype for secondary mirror alignment in telescopes," *Research in Astronomy and Astrophysics*, vol. 18, no. 9, p. 115, 2018.

[6] B. Nikolic, R. M. Prestage, D. S. Chandler, C. J. Hills, and R. E. Hills, "Out-of-focus holography at the Green Bank telescope," *Astronomy & Astrophysics*, vol. 465, no. 2, pp. 685–693, 2007.

[7] R. C. LaBelle and D. J. Rochblatt, "Calibration and performance measurements for the nasa deep space network aperture enhancement project (daep)," *Acta Astronautica*, vol. 147, pp. 37–47, 2018.

[8] J. X. Sun, Y. X. Zuo, J. Yang, J. M. Ma, and D. R. Lu, "Thermal deformation of the delingha 13.7 m telescope," *Acta Astronomica Sinica*, vol. 55, no. 3, pp. 246–255, 2014.

[9] Y. C. Jiang, J. Q. Wang, W. Gou, L. F. Yu, and Y. B. Jiang, "The measurement of sub-reflector's displacements of large radio telescopes by PSD method," *Acta Astronomica Sinica*, vol. 60, no. 6, pp. 98–107, 2019.

[10] Y. Hou, Y. Duan, Y. Dou et al., "Calibration of adjusting mechanism for subreflector of a 65 meters radio telescope," *China Mechanical Engineering*, vol. 24, 2013.

[11] J. Q. Wang, J. Zhang, Q. Fan et al., "Main reflector gravity deformation and sub-reflector position measurement for radio telescope based on interferometer," *Scientia Sinica Physica, Mechanica & Astronomica*, vol. 49, 2019.

[12] T. Pisanu, F. Buffa, R. Concu et al., "A PSD (position sensing device) to map the shift and tilt of the SRT secondary mirror," *Proceedings of SPIE*, vol. 9145, 2014.

[13] F. Buffa, A. Causin, A. Cazzani et al., "The Sardinia radio telescope: a comparison between close-range photogrammetry and finite element models," *Mathematics and Mechanics of Solids*, vol. 22, no. 5, 2017.

[14] C. S. Liu, Y. F. Pu, Y. T. Chen, and Y. T. Luo, "Design of a measurement system for simultaneously measuring six-degree-of-freedom geometric errors of a long linear stage," *Sensors*, vol. 18, no. 11, 2018.

[15] C. S. Liu, H. C. Hsu, and Y. X. Lin, "Design of a six-degree-of-freedom geometric errors measurement system for a rotary axis of a machine tool," *Optics and Lasers in Engineering*, vol. 127, Article ID 105949, 2020.

[16] Y. C. Sun, Y. J. Pang, and Z. X. Bai, "Application technology of laser triangulation," *Laser Journal*, vol. 42, no. 4, pp. 1–8, 2021.

[17] G. H. Wu, S. Y. Zhou, Y. T. Yang, and Ni. Kai, "Dual-comb ranging and its applications," *Chinese Journal of Lasers*, vol. 48, no. 15, pp. 250–267, 2021.

[18] N. Wang, "Xinjiang qitai 110 m radio telescope," *Scientia Sinica Physica, Mechanica & Astronomica*, vol. 44, no. 8, pp. 783–794, 2014.

[19] B. B. Xiang, C. S. Wang, and W. Wang, "Adjustment method of subreflector position of reflector antennas based on electromechanical couple theory," *Systems Engineering and Electronics*, vol. 40, no. 3, pp. 489–497, 2018.

[20] W. Xu, J. W. Li, and H. Zhang, "Hybrid total least squares for fitting spatial straight lines," *Geotechnical Investigation and Surveying*, vol. 47, no. 1, pp. 70–73, 2019.

[21] F. Zhang, J. Q. Wang, and H. Luo, "The comparative and analysis of seven - parameter coordinate conversion model," *Geomatics & Spatial Information Technology*, vol. 39, no. 5, pp. 48–51, 2016.